Size and Orientation of the Lipid II Headgroup As Revealed by AFM Imaging[†]

D. N. Ganchev,* H. E. Hasper, E. Breukink, and B. de Kruijff

Institute of Biomembranes, Department of Biochemistry of Membranes, Faculty of Chemistry, Utrecht University, Utrecht, The Netherlands

Received September 20, 2005; Revised Manuscript Received January 25, 2006

ABSTRACT: In this study, we investigated the size and orientation of the bacterial Lipid II (L II) headgroup when the L II molecule is present in liquid-crystalline domains of DOPC in a supported DPPC bilayer. Using atomic force microscopy, we detected that L II causes the appearance of a 1.9 nm thick layer, situated over the DOPC headgroup region. With an increased scanning force, this layer can be penetrated by the AFM tip down to the level of the DOPC bilayer. Using different L II precursor molecules, we demonstrated that the detected layer consists of the headgroups of L II and that the MurNAc−pentapeptide unit of the headgroup is responsible for the measured 1.9 nm height of that layer. Monolayer experiments provided information about the in-plane dimensions of the L II headgroup. On the basis of these results and considerations of the molecular dimensions of L II headgroup constituents, we propose a model for the orientation of the L II headgroup in the membrane. In this model, the pentapeptide of the L II headgroup is rather extended and points away from the bilayer surface, which could be important for biological processes, in which L II is involved.

The cell wall is an essential structure in bacteria, plays an important role in determining bacterial shape, and protects against osmotic stress. It consists of a cross-linked polysaccharide−peptide complex, called peptidoglycan, the building blocks of which are synthesized inside the cell as a part of a specific carrier molecule, called Lipid II (Figure 1A) (*1*). Lipid II (L II)[1] is a complex molecule (Figure 1B) containing a long polyisoprenyl (bactoprenyl) chain connected via a pyrophosphate to a large hydrophilic group, consisting of a disaccharide−pentapeptide unit, which is the building block for the synthesis of the peptidoglycan. The biosynthesis route of L II includes attachment to the phosphorylated bactoprenyl chain of an *N*-acetylmuramic acid (MurNAc) carrying a pentapeptide, resulting in the formation of Lipid I. Hereafter, an additional sugar, *N*-acetylglucosamine (GlcNAc), is attached to form a complete L II molecule. After the assembly on the cytosolic leaflet of the membrane, L II is translocated to the periplasmic side by an unknown mechanism, where the disaccharide−pentapeptide unit is incorporated in the cell wall. The phosphorylated bactoprenyl chain returns to the cytosolic leaflet for a new cycle of synthesis. The L II pool in an average cell turns out to be very small, the number of molecules being on the order of several hundreds to thousands per cell (*2*), but because of its high rate of turnover, this amount suffices to allow the peptidoglycan layer of bacteria to grow rapidly.

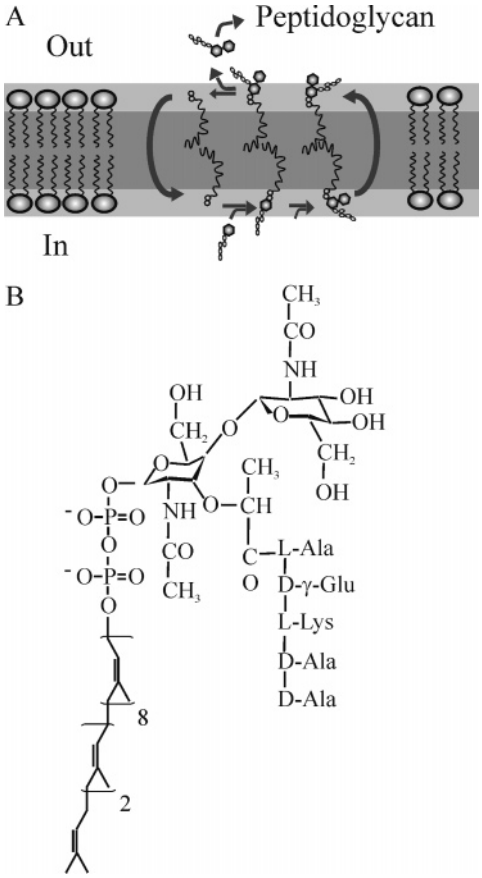

FIGURE 1: (A) Schematic representation of L II synthesis and function in a peptidoglycan synthesis. Different precursor molecules of L II, i.e., bactoprenyl phosphate, bactoprenyl pyrophosphate, and L I are depicted. (B) Chemical structure of L II.

The bacterial cell wall is a structure, specific for bacteria, and not present in higher organisms. This makes the cell

[†] This study was financially supported by a grant from NWO-CW.

* To whom correspondence should be addressed. E-mail: d.n.ganchev@gmail.com. Telephone: +1 216 3686718. Fax: +1 216 3683952.

[1] Abbreviations: AFM, atomic force microscopy; L II, Lipid II; L I, Lipid I; 11 P, bactoprenyl phosphate; 11 PP, bactoprenyl pyrophosphate; DOPC, 1,2-dioleoyl-*sn*-glycero-3-phosphocholine; DPPC, 1,2-dipalmitoyl-*sn*-glycero-3-phosphocholine; SUV, small unilamellar vesicles.

10.1021/bi051913e CCC: $33.50
Published on Web 04/25/2006

wall and the molecules involved in its synthesis ideal targets for bactericides. It was established that several antibiotics target specifically the L II molecule. Some of these antibiotics, such as mersacidin and vancomycin, prevent the synthesis of the cell wall by interacting with L II (*3*, *4*). Others like the lantibiotic nisin use L II as a receptor for targeted pore formation (*5*, *6*). Nisin and L II assemble into pores with defined composition (*6*, *7*) that permeabilize the membrane, thereby killing the bacteria.

The importance of the role of L II in cell wall synthesis and as a target of antibiotics strongly contrasts with the lack of knowledge about this intriguing biomolecule. This applies in particular to the orientation of the headgroup of L II when this molecule is present in a membrane. The headgroup of L II is crucially important for specific recognition by certain antibiotics (*8*). It was demonstrated that vancomycin binds to the last two residues in the pentapeptide (*9*), whereas the pyrophosphate moiety is essential for specific docking of nisin (*10*). This suggests that the orientation of the L II headgroup plays a significant role in this specific recognition. The proper utilization and incorporation of the headgroup in the peptidoglycan layer also will require a certain orientation of the carbohydrate−pentapeptide building block with respect to the membrane. Therefore, insights in the organization of the L II headgroup at the membrane will provide a better understanding of the processes of specific antibiotic recognition and cell wall synthesis. However, the complex structure of the L II polar headgroup, which includes a pentapeptide with an unusual amino acid composition (D-γ-Glu at position 2 and two D-Ala residues at positions 4 and 5), makes this structure rather difficult to characterize via direct structure-determining techniques such as NMR and X-ray diffraction.

AFM has proven to be a suitable technique for imaging and mechanically manipulating membranes and bilayers with nanometer resolution and in an aqueous environment (*11*, *12*). In this study, we applied AFM to supported lipid bilayers containing L II and L II precursors to gain insight into the surface organization of this molecule. To be able to facilitate imaging of L II, we made use of a bilayer of gel state lipids in which small domains of liquid-crystalline lipids are present. These domains are expected to contain fluid lipids such as L II, and they are readily identified by their lower height (*13*).

The data provide for the first time quantitative information about the size and orientation of the L II headgroup at the bilayer interface. We demonstrate that the L II headgroup protrudes ~1.9 nm over the headgroup region of the DOPC bilayer, where L II is located. This corresponds to a conformation with the pentapeptide pointing away from the bilayer surface.

MATERIALS AND METHODS

Lipids. 1,2-Dipalmitoyl-*sn*-glycero-3-phosphocholine (DPPC) and 1,2-dioleoyl-*sn*-glycero-3-phosphocholine (DOPC) were obtained from Avanti Polar Lipids (Alabaster, AL) and were dissolved at 20 mM in a mixture of methanol and chloroform (1:3, v/v). Synthesis of L II, L I, and bactoprenyl pyrophosphate (a generous gift from E. Swiezewska) was described elsewhere (*6*). The lysine form of UDP-MurNAc-pentapeptide was labeled with NBD-chloride at the lysine of the pentapeptide moiety residue in a manner identical to that described for the labeling of UDP-MurNAc-pentapeptide with pyrenesulfonyl chloride (*6*).

Nisin A was produced by batch fermentation, isolated, and purified as described previously (*14*). It was dissolved in a buffer solution [50 mM NaCl and 50 mM Na_3PO_4 (pH 6.8, adjusted with HCl)] at a concentration of 10 μM.

Preparation of Small Unilamellar Vesicles (SUV). SUV were prepared as described previously (*15*). Briefly, a mixture of lipids in the desired molar ratio was dried in a rotary evaporator, and the mixed films were stored overnight under high vacuum. All films were hydrated with a buffer, containing 50 mM NaCl and 50 mM Na_3PO_4, adjusted to pH 6.8 with HCl. This buffer was used throughout the study. The final lipid concentration was 1 mM. Ten freeze−thaw cycles were performed to obtain a suspension of large multilamellar vesicles. Subsequently, this suspension was sonicated in an ultrasound bath sonicator (Branson, Danburry, CT) at maximum power for 30 min, at 45 °C. Possible remaining large vesicles were spun down for 1 h at 20800*g* and 4 °C. The SUV suspension was used within 3 days, and the AFM results were not dependent on the time of storage.

Preparation of Supported Lipid Bilayers. The preparation of supported lipid bilayers was performed as described previously (*16*). Briefly, we deposited a 75 μL SUV suspension onto freshly cleaved mica (ϕ = 10 mm). The vesicles were left to adsorb on the mica for 1 h at room temperature. Subsequently, the sample was rinsed with 75 μL of the buffer solution (three times) and heated for 1 h at 65 °C. After cooling to room temperature, the sample was rinsed again with 75 μL of the buffer solution (three times).

Incubation with Nisin. In these experiments, we gently applied 75 μL of a 10 μM nisin solution over the preformed bilayer. This first volume was replaced with another 75 μL nisin solution, ensuring in this way a final concentration of the nisin over the bilayer of ~10 μM. The sample was left for 15 min at room temperature and then rinsed three times with 75 μL of the buffer solution to remove the nonadsorbed nisin.

AFM Imaging. The supported bilayers were covered by the buffer solution during the measurements. The samples were mounted on an E-scanner, which was calibrated on a standard grid, of a Nanoscope IIIa AFM instrument (Digital Instruments, Santa Barbara, CA). A fluid cell without an O-ring was fitted, and the sample was scanned in contact mode, using oxide-sharpened Si_3N_4 tips attached to a triangular cantilever with a spring constant of 0.06 N/m (NanoProbe, DI, Santa Barbara, CA). Imaging was performed at a minimal force (<0.5 nN) where the scans were stable and clear and at temperatures between 23 and 28 °C. In some cases, images were recorded at an increased scanning force.

Surface Pressure−Area Isotherms. Surface pressure−area (π−A) isotherms were obtained by compression of a spread lipid monolayer on a surface of a computer-driven Langmuir trough. Compression is performed by moving a Teflon barrier over the surface of the trough. The speed of the barrier was 3 cm/min, and the dimensions of the trough were 17.3 cm (width) × 35 cm (length). As a subphase, 50 mM NaCl and 50 mM Na_3PO_4, adjusted to pH 6.8, were used. The surface tension of the buffer was 71.2 mN/m. L II (20 nmol) from organic solvent (1:1 methanol/chloroform mixture) was carefully deposited on four to five different spots on the

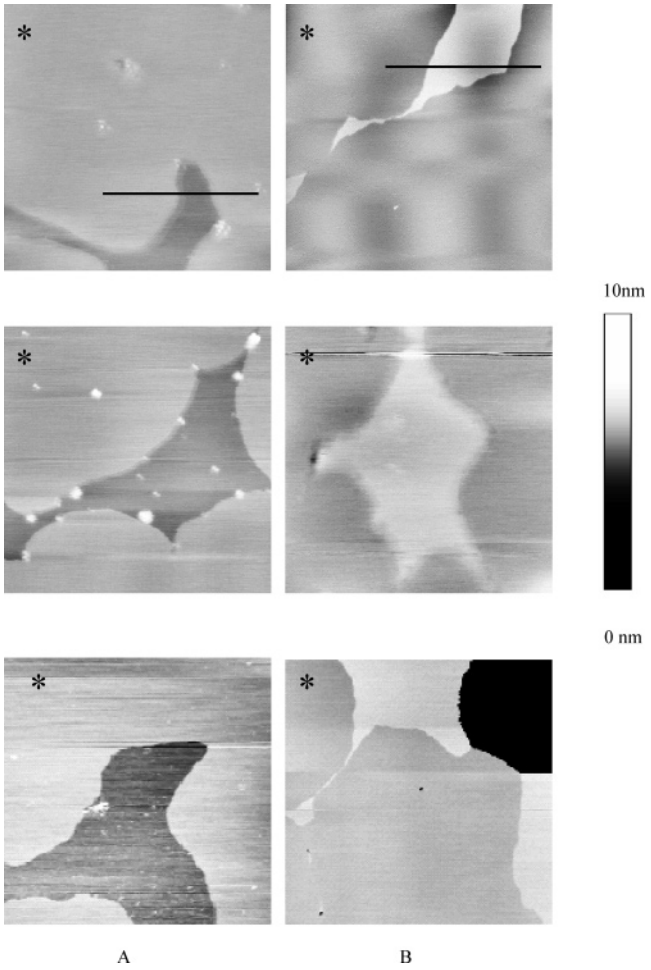

FIGURE 2: Series of typical AFM images of domains present in a supported mixed DOPC/DPPC (5:95 molar ratio) bilayer in the absence (A) and presence of L II (B). Images are taken from different bilayer preparations to demonstrate the reproducibility of the results. The L II:DOPC:DPPC ratio of the L II-containing sample is 2.5:2.5:95. All images are recorded with a low scanning force (<0.5 nN). The scan size in all cases is 2 μm × 2 μm, and the *z*-scale is 10 nm. In all images, the DPPC bilayer is marked with an asterisk.

surface of the trough. Before the start of the compression cycle, we waited 15 min for evaporation of the solvent. The initial surface pressure, at which the compression started, was 0 mN/m. Experiments were performed at room temperature (~22 °C).

RESULTS

Imaging the Effect of Incorporation of L II on DOPC Domains in a DPPC Bilayer. We initially selected the 5 mol % DOPC in DPPC mixed bilayer as the experimental system for our studies. The small liquid-crystalline domains of DOPC with a packing similar to that of biological membranes can be readily distinguished from the surrounding gel state DPPC bilayer because they are 0.76 ± 0.11 nm lower and therefore show up as darker in the AFM images (see the series of images in Figure 2A). When half of the DOPC in these samples is replaced with L II, again the typical phase separation pattern is observed as in the binary mixture (Figure 2B). However, in contrast to the DOPC/DPPC mixture, the domains are now 1.16 ± 0.14 nm higher than the surrounding DPPC bilayer and show up as lighter areas in the AFM

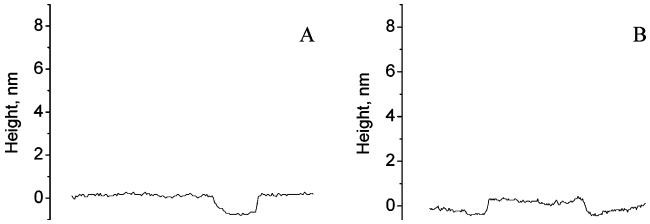

FIGURE 3: Height profiles of the bilayer surface of the images in column 1 of Figure 2, taken across the black lines in the images: (A) a height profile of a DOPC/DPPC bilayer and (B) a height profile of a L II/DOPC/DPPC bilayer with a low imaging force.

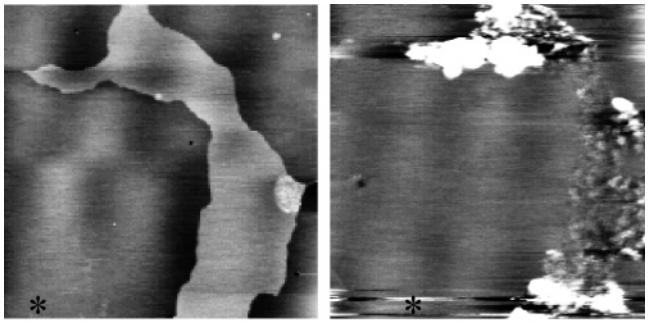

FIGURE 4: AFM images of domains in a L II/DOPC/DPPC bilayer at a molar ratio of2.5:2.5:95, before incubation with nisin (A) and after the incubation (B). The same domain is visualized in both images. The scanning force is minimized (~0.5 nN); the scan size is 5 μm × 5 μm, and the *z*-scale is 10 nm.

images. The thickness of the DPPC bilayer as measured at defects down to the mica (shown for instance in the bottom right panel of Figure 2) was 5.5−6.0 nm in all cases. These data suggest that L II is preferentially localized in DOPC domains and increases its thickness by ~1.9 nm when scanned at low force (~0.5 nN). To further describe the surfaces of the investigated bilayers, we made cross sections of the DOPC/DPPC and L II/DOPC/DPPC bilayers, using the AFM software. Typical height profiles are presented in Figure 3. To verify the localization of L II, we incubated the samples with the lantibiotic nisin that specifically interacts with L II. In the absence of L II, no changes were detected in the morphology of the sample (data not shown). However, in the L II-containing sample, the domains containing DOPC and L II were substantially perturbed (Figure 4). The overall contour of the domain was preserved, but the bilayer within the domain acquired a particulate structure with large local fluctuations in height, reaching heights up to 10−15 nm with respect to the DPPC. Apparently, the nisin−L II interaction causes a major reorganization within the L II-containing bilayer. We observed (data not shown) that part of the nisin is loosely bound to the domains because consecutive scanning results in removal of the higher aggregates in the DOPC/L II domain, most likely because some loosely adsorbed nisin was removed. These experiments demonstrate that L II is localized in the DOPC domains and that the presence of L II causes an increase in the height of these domains.

The L II/DOPC Domains Are Sensitive to the Applied Scanning Force. The force, which is applied on the AFM tip during scanning, usually is minimized down to ~0.5 nN to prevent damaging of the sample. However, we could increase this force in a controlled fashion to mechanically

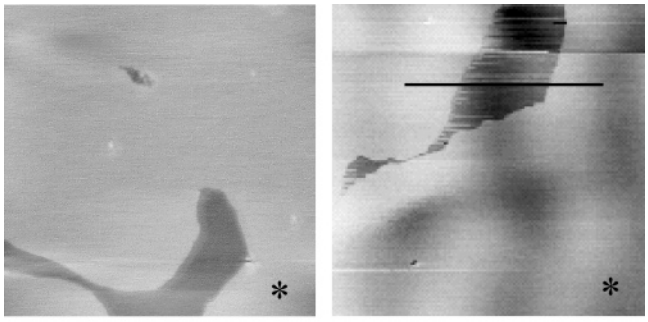

A B

FIGURE 5: AFM images of domains in DOPC/DPPC and L II/DOPC/DPPC bilayers recorded with a high scanning force (5−6 nN): (A) DOPC domains and (B) L II/DOPC domains. The scan size in both cases is 2 μm × 2 μm, and the *z*-scale is 10 nm. Note that the same areas as in Figure 2, first row, are visualized.

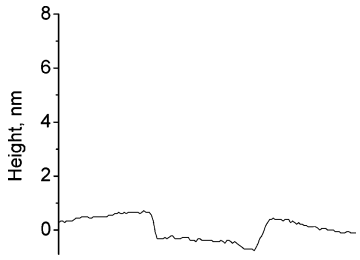

FIGURE 6: Height profile of a bilayer surface of a L II/DOPC/DPPC bilayer, taken across the black line in the image in Figure 5B at an elevated imaging force.

manipulate the sample. We exploited this ability of the AFM to further characterize the studied system. Therefore, we imaged both DOPC/DPPC and L II/DOPC/DPPC bilayers at an elevated scanning force. The AFM images of DOPC domains in DOPC/DPPC bilayers recorded with a 10-fold increase in the applied force were found to be similar to the images recorded with a low force (compare Figure 5A with Figure 2A, top panel). Only some debris was removed by the tip during scanning. However, the behavior of L II/DOPC/DPPC bilayers at an increased scanning force is strikingly different. With an approximately 10-fold increase in the applied force, the L II/DOPC domains are visualized 0.81 ± 0.15 nm lower than the surrounding DPPC bilayer (Figure 5B; compare the same domain in Figure 2B, top panel) instead of ∼1.16 nm higher. A height profile of the penetrated domain is presented in Figure 6. This process is completely reversible, and when the scanning force is decreased to 0.5 nN, the domains reappear and could be visualized again 1.16 ± 0.14 nm higher than the DPPC areas (data not shown). This procedure could be performed consecutively several times over the same spot without lipid material being carried away by the tip during these manipulations. These results demonstrate that in the DOPC/L II (1:1) domains the presence of L II causes the appearance of an ∼1.9 nm thick layer, situated over the DOPC headgroup region, which could be reversibly penetrated by the AFM tip down to the level of the surface of the DOPC bilayer.

Next, we were interested in determining the L II concentration at which the 1.9 nm thick layer would start to appear. Therefore, we varied the L II:lipid ratio and increased the DOPC:DPPC ratio to 1:9 to facilitate the detection of the L II/DOPC domains. At all investigated molar ratios, the thickness of the continuous DPPC bilayer is 5.5−6.0 nm.

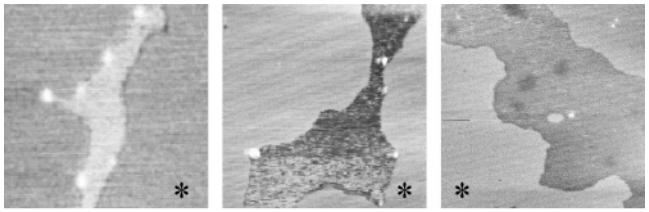

A B C

FIGURE 7: AFM images of L II/DOPC/DPPC domains at different L II:DOPC ratios. The (L II+DOPC):DPPC ratio in all cases was 10:90: (A) 1:14 L II:DOPC, (B) 1:19 L II:DOPC, and (C) 1:99 L II:DOPC. All images were recorded with a force of ∼0.5 nN. The scan size in all cases is 2 μm × 2 μm, and the *z*-scale is 10 nm.

At L II:DOPC molar ratios of 1:4.5 and 1:9, behavior very similar to that described for a molar ratio of 1:1 was found. L II/DOPC domains appeared 1.15 ± 0.20 nm higher than the DPPC bilayer, and they are stable upon scanning at a minimized force (data not shown). Increasing the scanning force resulted in penetration of the tip through the layer and subsequent visualization of lower domains (0.7 ± 0.2 nm). Tip penetration is completely reversible, and minimizing the force allows higher domains to be visualized. At a L II:DOPC ratio of 1:14, it is still possible to visualize elevated domains, but only with a minimal scanning force (<1 nN) (Figure 7A). At a still lower ratio of 1:19, elevated areas can be detected, but visualizing complete elevated domains is rather difficult since even at a slight increase in the force during scanning (due to a thermal drift in the AFM) the domains are imaged as lower areas with respect to the DPPC level (see the change in contrast in the domain, visualized in Figure 7B). Reducing the amount of L II to a molar ratio of <1:49 results in images in which the L II/DOPC domains have the typical appearance as in the absence of L II. We were unable to visualize elevated areas even at the lowest possible force, allowing stable imaging. A typical image of L II/DOPC domains at a 1:99 ratio is shown in Figure 7C. These experiments demonstrate that a certain L II:DOPC ratio of approximately 1:14 is needed to form elevated domains that can be stably imaged at low force but which are penetrated by the AFM tip down to the DOPC bilayer level with an increased force.

The Headgroup of L II Is Responsible for the Measured 1.90 nm Increase in the Bilayer Heights. We next tried to determine which part of the L II molecule causes the observed increase in the height of the DOPC domains. We systematically decreased the size of the L II group and studied L II precursors, incorporated in DOPC/DPPC bilayers. The precursor:DOPC:DPPC molar ratio was 1:9:90. All investigated precursor molecules contain the bactoprenyl chain, to which either one phosphate (11 P) or two phosphates (11 PP) are attached. L I differs from L II in that it lacks the last sugar (GlcNAc) in its hydrophilic headgroup (see Figure 1).

The behavior of L I/DOPC domains follows the pattern established for L II-containing domains. With a minimized scanning force, the domains are 1.21 ± 0.13 nm higher than the 5.5−6.0 nm thick DPPC bilayer (Figure 8A). With an increase in the scanning force, they are visualized as 0.74 ± 0.12 nm lower than the DPPC level, which amounts to a 1.95 nm thickness of the layer, present above the DOPC

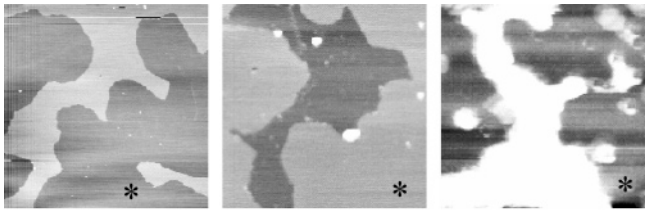

A B C

FIGURE 8: AFM images of domains in a 1:9:90 L I/DOPC/DPPC bilayer (A) and a 1:9:90 11 PP/DOPC/DPPC bilayer before (B) and after (C) incubation with nisin. All images were recorded with a minimal scanning force (<0.5 nN). The scan size in both cases is 5 μm × 5 μm, and the *z*-scale is 10 nm.

Table 1: Effect of L II and Some Analogues on the Height Differences between the DOPC Domains Where They Reside and the Surface of the Gel State DPPC Bilayer[a]

lipid mixture	no. of frames analyzed	height difference (nm) (mean ± standard deviation)
DOPC/DPPC, low force	10	−0.76 ± 0.11
L II/DOPC/DPPC, low force	20	1.16 ± 0.14
L II/DOPC/DPPC, high force	20	−0.81 ± 0.15
L I/DOPC/DPPC, low force	10	1.21 ± 0.13
L I/DOPC/DPPC, high force	10	−0.74 ± 0.12
11 PP/DOPC/DPPC, low force	20	−0.77 ± 0.16
L II-NBD/DOPC/DPPC, low force	5	1.22 ± 0.16
L II-NBD/DOPC/DPPC, high force	5	−0.76 ± 0.14

[a] The data were obtained from the experiments described in the legends of Figures 2−6. At least three different samples were analyzed for each system.

headgroup level. This process is reversible, and minimizing the scanning force allows visualization of higher domains.

When we imaged systems containing only the bactoprenyl chain with attached phosphate or pyrophosphate groups (11 P or 11 PP, respectively), we were not able to detect higher domains with respect to the DPPC bilayer. In all experiments, only lower domains were observed, even at the minimal force needed for stable scanning (Figure 8B). The thickness of the DPPC bilayer remained 5.5−6.0 nm, and the 11 P (or 11 PP)/DOPC domains were ∼0.77 ± 0.16 nm lower than the surrounding DPPC bilayer. Experiments with nisin decoration were performed over both L I/DOPC/DPPC and 11 PP/DOPC/DPPC bilayers. Nisin, which is positively charged, was shown to aspecifically interact with negatively charged lipids (*18*). After the incubation with nisin, elevations irregular in height were observed in both cases (Figure 6C depicts a 11 PP/DOPC domain after nisin incubation), instead of lower areas, which confirms the presence of the respective precursor molecules in the observed domains.

The differences in height between the L II (precursor)/DOPC domains and the surrounding DPPC bilayer are summarized in Table 1.

The performed experiments demonstrated that the increase in the height of L II/DOPC domains is presumably caused by the *N*-acetylmuramic acid−pentapeptide part of the L II headgroup.

The Increased Height Is Not an Artifact Caused by Electrostatic Interactions between the AFM Tip and the Lipid Headgroup. In principle, it is possible that the charged lysine residue in the pentapeptide of the L II headgroup interacts electrostatically with the AFM tip. This could affect the height differences which we measure for L II in DOPC domains. To check this possibility, we imaged supported bilayers, containing a L II analogue, in which the charged lysine was blocked with a NBD group. The used L II-NBD:DOPC:DPPC molar ratio was 1:9:90. Phase-separated domains, 1.22 ± 0.16 nm higher than the surrounding DPPC bilayer, were imaged with a minimized scanning force (Table 1). These domains are sensitive to an increase in the scanning force, following in their behavior the pattern, similar to that observed for the parent molecule. With imaging at an increased force, the tip scans over the DOPC headgroup level, 0.76 ± 0.14 nm below the DPPC bilayer (Table 1). These experiments demonstrate that the charge of the lysine residue does not influence the measured height differences, and this makes it unlikely that electrostatic interactions between the AFM tip and the sample play a role in causing the increased height of the DOPC/L II domains.

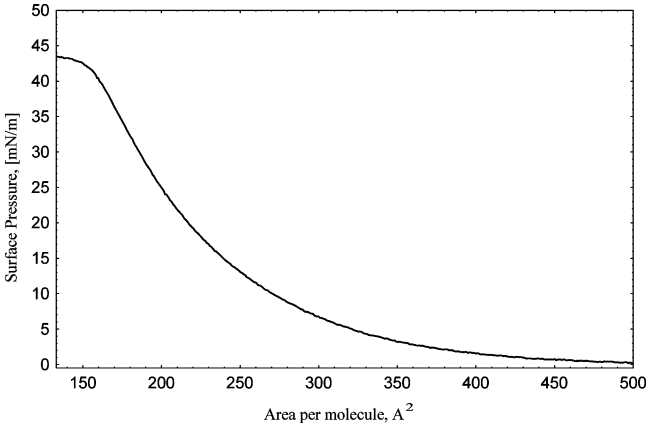

FIGURE 9: Pressure−area isotherms for a L II monolayer spread over a buffer solution in a Langmuir trough.

The Headgroup of L II Has a Limiting Area of ∼1.5 nm^2. So far, we have determined the height of the L II headgroup with respect to the surface of the bilayer. To completely characterize the size of the headgroup, we need to know the area that a L II molecule occupies in a bilayer. We can estimate this area by determining the limiting area of L II in a monolayer, spread on a buffer surface. We performed monolayer compression experiments in a Langmuir trough and determined the limiting area per molecule and collapse pressure for a pure L II monolayer, spread on a buffer surface. In separate runs, we obtained reproducible $\pi-A$ isotherms with limiting areas of ∼1.5 nm^2 and a collapse pressure of 43.5 mN/m (Figure 9).

DISCUSSION

The aim of this study was to provide information about the size and orientation of the headgroup of L II. We used a combination of AFM imaging and force manipulation to fully characterize the dimensions of the headgroup. The obtained results revealed that the L II headgroup protrudes ∼1.9 nm from the DOPC level bilayer and forms a layer that is stable at a minimized scanning force. Using L II precursor molecules (L I and 11 PP), we demonstrated that this height increase is due to the *N*-acetylmuramic acid−pentapeptide part of the L II headgroup. We fully described the size of the L II headgroup by determining the limiting area per molecule in a spread monolayer to be 1.5 nm^2.

Here we will discuss the imaging mechanism which determines the observed heights of L II/DOPC domains at

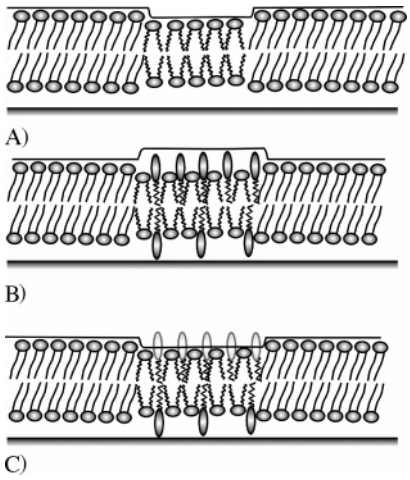

FIGURE 10: Position of the AFM tip over domains of different composition in L II/DOPC/DPPC supported bilayers. The height profile (position of the tip) is shown with a thick line: (A) pure DOPC domains with scanning at a minimal force and (B) L II/DOPC/DPPC domains imaged with a low force, where the tip scans were taken over the L II headgroups. (C) With an increased scanning force, the tip penetrates through the L II headgroup region and scans over the DOPC headgroups.

minimized and increased scanning forces, and after discussing the possible effect of electrostatic interaction on the measurements, we will describe the orientation of L II headgroup, using the data for the headgroup dimensions.

In our experiments, we demonstrated that the fluid state bactoprenyl chain of L II co-separates in the liquid-crystalline DOPC domains, most probably due to the squeezing out of the fluid L II acyl chain from the highly ordered gel state bilayer. Therefore, we postulate that over the DOPC domains the tip scans over the headgroup region of L II and when the force increases, it penetrates through it down to the DOPC headgroup level (see Figure 10). In the presented cross sections, we could see that the surface of both nonpenetrated and penetrated L II domains could not be distinguished from the surfaces of the conventional DOPC or DPPC areas. Interestingly, in contrast to the irreversible damaging of the lipid bilayers with an increased scanning force (*17*), in our experiments the imaged L II-containing domains are restored to their initial height once the scanning force is minimized. This demonstrates that L II molecules are not removed by the tip with an increased scanning force, which is an indication of their stable anchoring within the DOPC bilayer.

Another characteristic feature observed in our experiments is the fact that after the penetration through the L II headgroup level, the tip scans over the DOPC headgroup level. What is the explanation of this unusual behavior? Obviously, there is a difference between the scanning forces, which each of the headgroup layers could withstand. At a 1:1 L II:DOPC molar ratio, a force of ~4−5 nN is sufficient for penetration through the L II headgroup level, and this force decreases with the decrease in the L II molar ratio.

In the literature, there are several reports about the forces needed to penetrate through a supported bilayer which range from 5−20 nN for different liquid crystalline bilayers to 20−30 nN for the more ordered gel state bilayers (*18*−*21*). If we assume that the tip radii are similar in all cases, then we can conclude that our value of ~5 nN for penetration of the L II layer down to the DOPC headgroup level is in good agreement with these studies. Why is it easier to penetrate through the L II headgroup layer than through a DOPC headgroup bilayer? The simplest explanation is that the L II headgroup layer is much looser. The L II headgroups are charged and thereby will repel each other, resulting in weaker cohesion and a layer that is easier to penetrate. This latter interpretation is supported by studies which showed that bilayers of charged lipids are more easily penetrated than noncharged bilayers (*18*).

The "penetration depth", defined as the height difference between nonpenetrated and penetrated L II/DOPC domains, is a measure of some characteristic dimension of the large L II headgroup. Here we discard the possibility that some part of the L II hydrocarbon chain could contribute to the measured height differences due to the fact that the position of phosphate groups in a bilayer, determined for other lipids, is quite well defined (*22*). Moreover, exposure of the hydrocarbon area to the polar environment of the interface would require a large unfavorable energy, which is found to be between 20 and 40 kcal mol^{-1} $Å^{-2}$ (*23*, *24*). This reasoning supports our hypothesis (evidences for which we provided with our precursor experiments) that the measured height increase is caused by the L II headgroup alone.

In principle, it could be argued that the positively charged lysine (the third amino acid residue in the pentapeptide) could interact with the negatively charged tip, influencing in this way the measured height differences. However, we can safely exclude this possibility because blocking the charge on the lysine with NBD did not affect the height difference. Furthermore, the presence of negative charges on 11 P and 11 PP within DOPC domains did not change the observed ~0.7−0.8 nm height difference between DPPC and the DOPC domains in which these molecules are localized. The absence of an electrostatic contribution to the measured height may be explained by the high ionic strength of the buffer solution that is used. The presence of 50 mM sodium chloride and 50 mM sodium phosphate screens to a large extent the electrostatic interactions.

These considerations lead us to conclude that the measured height of 1.9 nm is caused by the L II headgroup. What could be the conformation of the L II headgroup that is consistent with this dimension? An important indication is provided by a comparison between height measurements of L II and L I. Since we observed very similar heights for these lipids, we can conclude that the 1.9 nm height difference is due to the pentapeptide and the MurNAc to which the peptide is attached.

The estimated vertical dimension of the L II headgroup (1.9 nm) suggests that it is not very probable that the pentapeptide is oriented with its backbone lying flat over the bilayer surface because the average diameter of the peptide backbone and the side chains can be estimated to be much less than 1.9 nm. Therefore, we propose that the headgroup adopts a configuration in which the pentapeptide in an extended conformation points away from the bilayer. If we assume a rise per residue of 0.35 nm (as in a β-sheet conformation), a total length of ~1.4 nm can be estimated for the pentapeptide. To this number can be added the contributions due to the MurNAc and the -O-CH-CO- motif which connects the pentapeptide to this sugar, which together can be roughly estimated to contribute between 0.3 and 0.6 nm to the total height. This gives us a height of the L II

headgroup of 1.7−2.0 nm, which closely matches the value of 1.9 nm measured by AFM.

The $\pi-A$ isotherms give us the area occupied by the L II molecule in a monolayer. Not surprisingly, with the bulky headgroup of L II in mind, this area of 1.5 nm^2 is more than twice the area occupied by the PC molecule in a liquid-crystalline bilayer (*25*). The collapse pressure is comparable to the collapse pressures reported for other lipids (*26*). No phase transition was observed, and the monolayer remains in a liquid-expanded state during the whole compression cycle. Interestingly, the surface pressure starts to rise at an area per lipid molecule of ∼4.5 nm^2, which indicates a long-range interaction. The origin of this interaction could be either the electrostatic repulsion between the headgroups (suppressed by the salt ions in the buffer but still detectable in this type of experiment) or an entropic contribution from the highly disordered bactoprenyl chain. We did not investigate this issue further since this is out of the scope of this study.

A rough estimation of the size of the two sugar rings (assuming 0.15 nm between C atoms forming the C−C bond) is ∼0.1 nm^2 per sugar ring. This value is close to the values which could be inferred from relevant studies on glycolipids containing different numbers of sugar rings (*27*−*29*). In these studies, the limiting area per molecule for different glycolipids was found to increase ∼0.05−0.15 nm^2 for each sugar ring. For the case of glycolipid GD3, containing four sugar rings in its headgroup, the limiting area per molecule was found to be ∼0.9 nm^2 (*30*), while lactosyl ceramide occupies an area slightly smaller than that of a SM molecule with the same length of acyl chains (*31*). These studies also suggest that the sugar rings can have different orientations with respect to the surface of the bilayer, which results in differences in the area per each ring. Obviously, in our case, the area of both sugars (assuming that they lie flat on the bilayer surface and thus occupy a maximal possible area) could not account for the 1.5 nm^2 limiting area per molecule. Therefore, we postulate that the pentapeptide determines the large area occupied by the L II molecule. The measured limiting area per molecule suggests a radius of the pentapeptide at a cross section, determining this area to be ∼0.7 nm. We observed that below a L II:DOPC ratio of approximately 1:14 the AFM tip starts to penetrate the L II/DOPC domains at lower forces. It can be calculated from the cross-sectional areas of L II and DOPC [0.45 nm radius (*31*)] that at this concentration there are not enough L II molecules to form a tightly packed L II headgroup layer, even when it is assumed that all L II molecules are in the leaflet, facing the tip. So we could speculate that tight packing (or nearly tight packing) of L II headgroups is needed to withstand the pressure exerted by the scanning AFM tip at a minimized force.

In summary, we point out that we provided for the first time information about the size and orientation of the L II headgroup when this molecule is incorporated within a membrane-mimicking liquid-crystalline bilayer. On the basis of the data that were obtained, we proposed that the pentapeptide of the L II headgroup adopts a configuration pointing away from the bilayer surface and is rather extended. This could be important in the specific recognition by antimicrobial peptides and for peptidoglycan synthesis.

REFERENCES

1. van Heijenoort, J. (1994) in *Bacterial Cell Wall*, Elsevier, Amsterdam.
2. Kramer, N. E., Smid, E. J., Kok, J., de Kruijff, B., Kuipers, O. P., and Breukink, E. (2004) Resistance of Gram-positive bacteria to nisin is not determined by lipid II levels, *FEMS Microbiol. Lett. 239* (1), 157−161.
3. Brötz, H., Bierbaum, G., Leopold, K., Reynolds, P. E., and Sahl. H.-G. (1998) The Lantibiotic Mersacidin Inhibits Peptidoglycan Synthesis by Targeting Lipid II, *Antimicrob. Agents Chemother. 42*, 154−160.
4. Sheldrick, G. M., Jones, P. G., Kennard, O., Williams, D. H., and Smith, G. A. (1978) Structure of vancomycin and its complex with acetyl-D-alanyl-D-alanine, *Nature 271*, 223−225.
5. Breukink, E., Wiedemann, I., van Kraaij, C., Kuipers, O. P., Sahl, H.-G., and de Kruijff, B. (1999) Use of the cell wall precursor lipid II by a pore-forming peptide antibiotic, *Science 286* (5448), 2361−2364.
6. Breukink, E., van Heusden, H. E., Vollmerhaus, P. J., Swiezewska, E., Brunner, L., Walker, S., Heck, A. J., and de Kruijff, B. (2003) Lipid II is an intrinsic component of the pore induced by nisin in bacterial membranes, *J. Biol. Chem. 278*, 19898−19903.
7. Hasper, H. E., de Kruijff, B., and Breukink, E. (2004) Assembly and stability of nisin-lipid II pores, *Biochemistry 43*, 11567−11575.
8. Hoffmann, A., Pag, U., Wiedemann, I., and Sahl, H.-G. (2002) Combination of antibiotic mechanisms in lantibiotics, *Farmaco 57*, 685−691.
9. Bonev, B. B., Breukink, E., Swiezewska, E., de Kruijff, B., and Watts, A. (2004) Targeting extracellular pyrophosphates underpins the high selectivity of nisin, *FASEB J. 18* (15), 1862−1869.
10. Hsu, S. T., Breukink, E., Tischenko, E., Lutters, M. A., de Kruijff, B., Kaptein, R., Bonvin, A. M., and van Nuland, N. A. (2004) The nisin-lipid II complex reveals a pyrophosphate cage that provides a blueprint for novel antibiotics, *Nat. Struct. Mol. Biol. 11*, 963−967.
11. Müller, D. J., Kessler, M., Oesterhelt, F., Möller, C., Oesterhelt, D., and Gaub, H. (2002) Stability of Bacteriorhodopsin α-Helices and Loops Analyzed by Single-Molecule Force Spectroscopy, *Biophys. J. 83*, 3578−3588.
12. Dufrene, Y. F., Boland, T., Schneider, J. W., Barger, W. R., and Lee, G. U. (1998) Characterization of the physical properties of model biomembranes at the nanometer scale with the atomic force microscope, *Faraday Discuss. 111*, 79−94.
13. Ganchev, D. N., Rijkers, D. T. S., Snel, M. M. E., Killian, J. A., and de Kruijff, B. (2004) Strength of Integration of Transmembrane α-Helical Peptides in Lipid Bilayers As Determined by Atomic Force Spectroscopy, *Biochemistry 43*, 14987−14993.
14. Kuipers, O. P., Rollema, H. S., Yap, W. M., Boot, H. J., Siezen, R. J., and de Vos, W. M. (1992) Engineering dehydrated amino acid residues in the antimicrobial peptide nisin, *J. Biol. Chem. 267*, 24340−24346.
15. Mou, J., Czajkowsky, D. M., and Shao, Z. (1996) Gramicidin A aggregation in supported gel state phosphatidylcholine bilayers, *Biochemistry 35*, 3222−3226.
16. Rinia, H. A., Kik, R. A., Demel, R. A., Snel, M. M. E., Killian, J. A., van der Eerden, J. P. J. M., and de Kruijff, B. (2000) Visualization of Highly Ordered Striated Domains Induced by Transmembrane Peptides in Supported Phosphatidylcholine Bilayers, *Biochemistry 39*, 5852−5858.
17. Rinia, H. A., Demel, R. A., van der Eerden, J. P. J. M., and de Kruijff, B. (1999) Blistering of langmuir-blodgett bilayers containing anionic phospholipids as observed by atomic force microscopy, *Biophys. J. 77*, 1683−1693.
18. Künneke, S., Krüger, D., and Janshoff, A. (2004) Scrutiny of the Failure of Lipid Membranes as a Function of Headgroups, Chain Length, and Lamellarity Measured by Scanning Force Microscopy, *Biophys. J. 86*, 1545−1553.
19. Franz, V., Loi, S., Müller, H., Bamberg, E., and Butt, H.-J. (2002) Tip penetration through lipid bilayers in atomic force microscopy, *Colloids Surf., B 23* (2−3), 191−200.
20. Loi, S., Sun, G., Franz, V., and Butt, H.-J. (2002) Rupture of molecular thin films observed in atomic force microscopy. II. Experiment, *Phys. Rev. E 66*, 031602-1−031602-6.
21. Grant, L. M., and Tiberg, F. (2002) Normal and Lateral Forces between Lipid Covered Solids in Solution: Correlation with Layer Packing and Structure, *Biophys. J. 82*, 1373−1385.

22. White, S. H., and Wimley, W. C. (1999) Membrane protein folding and stability: Physical principles, *Annu. Rev. Biophys. Biomol. Struct. 28*, 319−365.
23. Reynolds, J. A., Gilbert, B. D., and Tanford, C. (1974) Empirical Correlation between Hydrophobic Free Energy and Aqueous Cavity Surface Area, *Proc. Natl. Acad. Sci. U.S.A. 71*, 2925−2927.
24. Hermann, R. B. (1977) Use of Solvent Cavity Area and Number of Packed Solvent Molecules around a Solute in regard to Hydrocarbon Solubilities and Hydrophobic Interactions, *Proc. Natl. Acad. Sci. U.S.A. 74*, 4144−4145.
25. Smaal, E. B., Mandersloot, J. G., Demel, R. A., de Kruijff, B., and de Gier, J. (1987) Consequences of the interaction of calcium with dioleoylphosphatidate-containing model membranes: Calcium-membrane and membrane-membrane interactions, *Biochim. Biophys. Acta 897*, 180−190.
26. Dynarowicz-Łątka, P., and Hąc-Wydro, K. (2004) Interactions between phosphatidylcholines and cholesterol in monolayers at the air/water interface, *Colloids Surf., B 37*, 21−25.
27. Filek, M., Gzyl, B., Laggner, P., and Kriechbaum, M. (2005) Effect of indole-3-acetic acid on surface properties of the wheat plastid lipids, *J. Plant Physiol. 3*, 245−252.
28. Heywang, C., Mathe, G., Hess, D., and Sackmann, E. (2001) Interaction of GM_1 glycolipid in phospholipid monolayers with wheat germ agglutinin: Effect of phospholipidic environment and subphase, *Chem. Phys. Lipids 113*, 41−53.
29. Maggio, B. (2004) Favorable and unfavorable lateral interactions of ceramide, neutral glycosphingolipids and gangliosides in mixed monolayers, *Chem. Phys. Lipids 132* (2), 209−224.
30. Diociaiuti, M., Ruspantini, I., Giordani, C., Bordi, F., and Chistolini, P. (2004) Distribution of GD3 in DPPC monolayers: A thermodynamic and atomic force microscopy combined study, *Biophys. J. 86*, 321−328.
31. Li, X.-M., Momsen, M. M., Brockman, H. L., and Brown, R. E. (2002). Lactosylceramide: Effect of Acyl Chain Structure on Phase Behavior and Molecular Packing, *Biophys. J. 83*, 1535−1546.

BI051913E